RAPID COMMUNICATION

Selective loss tailoring of broad-area diode lasers

Japanese Journal of Applied Physics **60**, 020901 (2021) **RAPID COMMUNICATION**
https://doi.org/**10.35848/1347-4065/abd70c**

Selective loss tailoring of broad-area diode lasers

Jiaxin Su[1,2], Cunzhu Tong[1*], Lijie Wang[1], Yanjing Wang[1], Huanyu Lu[1], Jun Wang[3], Shaoyang Tan[3], Sensen Li[4], Hangyu Peng[1], and Lijun Wang[1]

[1]*State Key Laboratory of Luminescence and Applications, Changchun Institute of Optics, Fine Mechanics and Physics, Chinese Academy of Sciences, Changchun 130033, People's Republic of China*
[2]*Center of Materials Science and Optoelectronics Engineering, University of Chinese Academy of Sciences, Beijing 100049, People's Republic of China*
[3]*Suzhou Everbright Photonics Co., Ltd., Suzhou 215000, People's Republic of China*
[4]*Science and Technology on Electro-Optical Information Security Control Laboratory, Tianjin 300308, People's Republic of China*

[*]E-mail: tongcz@ciomp.ac.cn

Received November 17, 2020; revised November 25, 2020; accepted December 27, 2020; published online January 19, 2021

High-power high-brightness broad-area diode lasers have poor lateral beam quality, which has limited the application range of this kind of device. To improve the lateral beam quality, a sawtooth microstructure laser was proposed and the microstructures were carefully designed according to the profiles of each lateral mode and their dependence on the self-heating induced thermal lens effect. As a result of selective mode loss adjustment, a 42% improvement in lateral beam quality was achieved under the power-maintained condition. This technology enables us to develop high-brightness direct-diode laser systems. © 2021 The Japan Society of Applied Physics

Due to their compact size and high efficiency, there has been a growing demand for high-power diode lasers to be used in pumping,[1–3] display,[4] material processing,[5] sensing[6] and medical[7] applications. These applications need lasers with high brightness, which is jointly dependent on the laser power and beam quality. Broad-area diode lasers (BALs) are the most important type of commercial diode lasers due to their high output power and simple manufacturing process. However, their wide emitter size and low mode discrimination in the lateral direction easily lead to multi-mode operation, which results in poor beam quality and low brightness, limiting their direct application.[8] Therefore, considerable effort has been made to improve the beam quality of diode lasers while sustaining high power and efficiency.

The lateral waveguiding of diode laser is influenced by various physical mechanisms, such as etched-ridge or trench-induced index guiding,[9] thermal lens induced by self-heating,[10] inhomogeneous carrier distribution, vertical epitaxial layer design, longitudinally varying optical power, etc.[11–13] Under high-power operation, BALs suffer from enhanced lateral index guiding, which supports additional high-order lateral modes. The lasing of higher-order modes with wider near field and wider far field will degrade both beam quality and total far-field angle, which is commonly referred to as far-field blooming.[12,13] For specific diode laser chips, lateral thermal lensing and current spreading play the most critical role in far-field blooming. As the injection current increases, more heating occurs, leading to larger lateral temperature gradient and corresponding index step. The near field of each mode would shrink and the enhanced overlap with electrically pumped region increases the gain of high-order modes. Simultaneously, lateral current spreading increases carrier accumulation near the stripe edges, providing more gain to high-order modes.[14] Therefore, more lateral modes will be supported due to equalized mode gain, causing wider far fields and deteriorated beam quality.

To improve the beam quality of diode laser, several approaches for reducing the number of lasing lateral modes have been proposed. One method is thermal path engineering in order to reduce the lateral temperature gradient and thus the thermal lensing effect.[15] It has been demonstrated that the lateral divergence can be lowered by reducing the thermal resistance of lasers or utilizing pedestal heat sinking for anti-guiding.[16] Furthermore, uniform gain profile and improved optical field stabilization can be achieved due to the suppression of current spreading by proton implantation or tailoring the current injection path.[17–22] Another effective way is introducing mode filters to produce extra loss for high-order modes, such as reducing the stripe width, tapered laser,[23,24] titled cavity,[25] inhomogeneous waveguide,[26] microstructure[27,28] and on-chip transverse Bragg grating.[29] All these lateral structuring techniques have improved the far-field divergence and beam quality of diode lasers due to enhanced mode discrimination. However, the challenge is to enhance the beam quality without compromising the laser efficiency and power by simple fabrication processing.

In this paper, a microstructure consisting of sawtooth-shaped arrays to improve the lateral beam quality of a typical BAL is proposed. The sawtooth microstructures produce selective propagation loss for different-order lateral modes through adjusting their shape and position. Higher-order modes can be suppressed due to larger loss under high current, while the impact on the low-order mode is low due to thermal-induced mode field shrinkage. The details of the sawtooth laser (STL) structure and its operating principle are first revealed. Then, the power characteristics and spatial beam properties of the structured lasers are described and compared with standard BALs from the same wafer. Analyses of laser characteristics have shown an obvious improvement in lateral beam quality without reducing the output power and efficiency.

Figure 1 shows the schematic view of the STL, which consists of four-array triangle microstructures symmetrically located near the corners of the laser mesa. Each isosceles triangle has a base of 5 μm and a height of 20 μm, 20 μm away from the facet. These etched holes provide additional optical loss due to light diffraction, scattering and absorption, which increases from the center to the stripe edges. As the modal near field broadens with the mode order, high-order modes exhibit a larger propagation loss than that of low-order modes, due to the increased overlap of their optical field with the lossy region. With increasing current, additional index guiding caused by thermal lensing tends to narrow the lateral near field of each mode, which is more prominent in the low-order modes. Therefore, such variational mode power in the

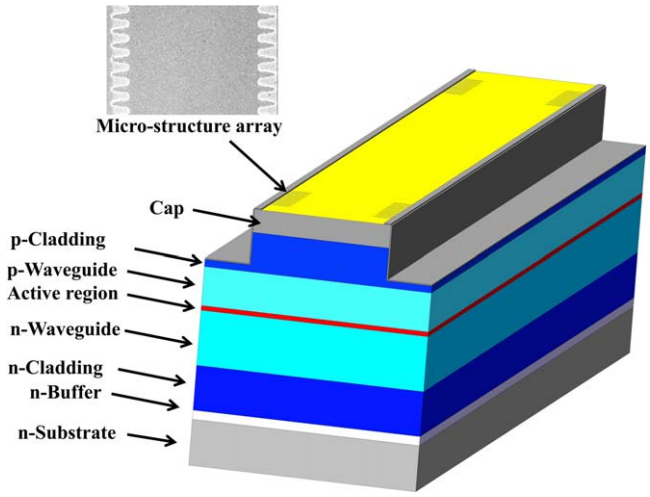

Fig. 1. (Color online) Schematic diagram of the STL.

structured region only allows the low-order modes to propagate, resulting in a reduced number of guided lateral modes.

Figures 2(a) and 2(b) show the calculated mode distribution of the fundamental mode (mode 0) and 9th high-order mode under the influence of the thermal lens effect.[11] The average thermal index change is $dN/dT = 3 \times 10^{-4}\,\mathrm{K}^{-1}$.[13] As can be seen, its near-field width shrinks when the refractive-index difference between the center and stripe edges of the laser increases. Similar effects can be expected for other modes. Subsequently, new high-order modes can be supported due to increased overlap with the electrically pumped region, degrading the beam quality. For the STL, enhanced heat-induced index gradient can push the optical field away from the lossy-structured region, reducing the modal loss as the current increases. However, high-order modes, which have strong optical intensity near the stripe edges, still suffer large loss induced by the sawtooth microstructure. As a result of enhanced mode discrimination, the lateral beam quality can be improved at high currents.

Figure 2(c) shows the relative optical loss of the microstructures for different-order lateral modes depending on the refractive-index gradient (Δn) caused by the thermal lens. $\Delta\alpha$ represents the ratio between the loss intensity induced by the microstructures and the mode intensity for different modes, which is defined as $I_0 - I_r/I_0$. I_0 and I_r represent the traveling optical energy before and after the microstructures, respectively, and higher $\Delta\alpha$ means more mode loss. From the dependence, it can be seen that the loss of each mode reduces with increasing Δn due to optical field shrinkage by thermal lens effect. The higher the lateral mode order, the larger the $\Delta\alpha$. Meanwhile, the effect is more impactful for high-order modes with increasing Δn. For example, the mode with order larger than 7 still suffers large propagation loss for Δn up to 0.0015, while the $\Delta\alpha$ of the fundamental mode keeps very low due to little mode power in the structured region. In this case, the selective loss-tailoring delays the lasing of high-order lateral modes, resulting in improved far-field and beam quality.

The laser epitaxial structure makes use of an asymmetric super-large optical cavity design for emission at 935 nm, which was grown on an n-type (001) GaAs substrate by metal

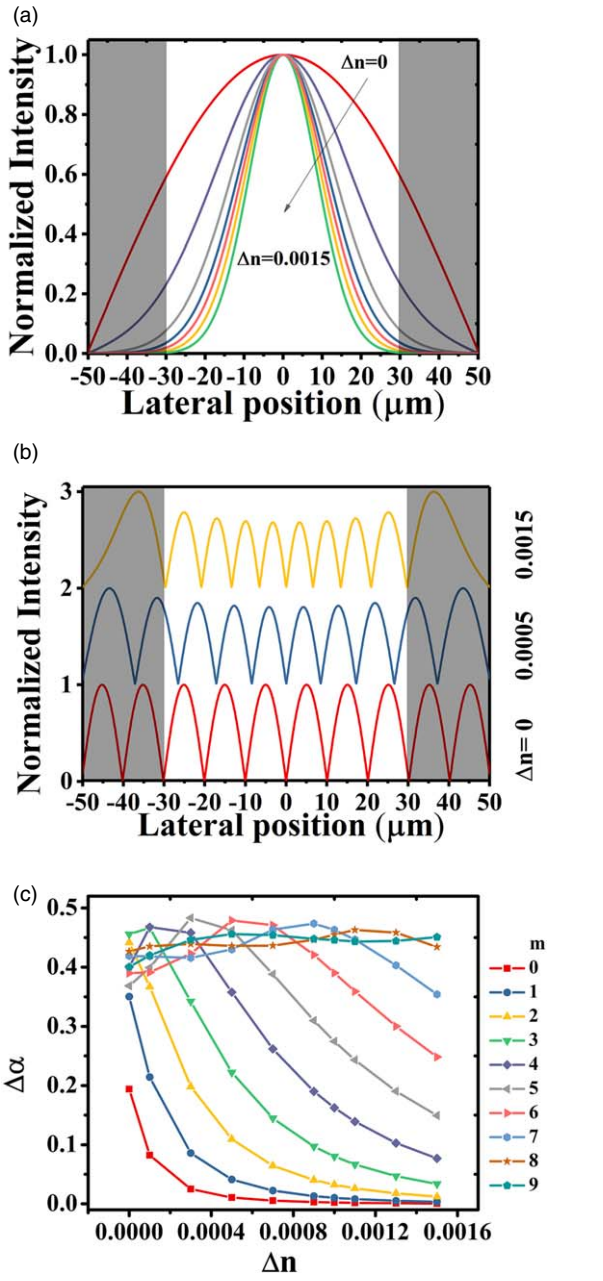

Fig. 2. (Color online) (a), (b) Calculated near-field profile of the fundamental lateral mode and 9th high-order mode as a function of heat-induced refractive-index change; (c) calculated light propagation loss versus the index difference for the lateral mode with different mode orders.

organic chemical vapor deposition. After wafer growth, a 100 μm wide mesa with sawtooth microstructures was formed by photolithography and etched together by inductively coupled plasma. The etching depth was down to the partial p-cladding layer (effective index step caused by etching is 10^{-3} level). Then, a 200 nm SiO_2 electrical insulating layer was deposited at 300 °C by plasma-enhanced chemical vapor deposition, and a 90 μm wide contact window was opened by reactive ion etching. After that, p-side metal contact deposition, backside thinning, polishing and n-metallization were performed. Finally, the wafer was cleaved into individual laser chips with a cavity length of 1.5 mm. For the experimental characterization, single emitters were bonded p-side down on C-mount copper heatsinks using an indium solder without facet coating and passivation.

Conventional BALs without microstructures were also fabricated from the same wafer for comparison.

The power-current–voltage characteristics of the STLs and BALs under CW operation at 20 °C are presented in Fig. 3. As can be seen, the voltage of the STL is comparable to that of the BAL. These lasers with 1.5 mm length were driven to 4 A, with similar current density and heating comparable to commercial 4 mm long laser at 10 W output power. The output power is slightly reduced by the introduction of sawtooth microstructures (from 3.76–3.66 W), with a difference of less than 3%. The peak efficiency of the STL and BAL is 49.2% and 49.8%, respectively, indicating that the microstructure causes negligible power degradation of the laser. This is because the microstructures only induce extra loss for high-order modes, especially under high injection current. The suppression of high-order modes allowed for the reduction of mode competition, which is beneficial for achieving improved slope efficiency.[27,28)]

Figures 4(a) and 4(b) show the measured near-field profiles at 1 A/4 A and near-field widths versus the injection current for both kinds of lasers (using BP209-VIS Scanning-Slit Optical Beam Profiler and a 20X-objective). With the increase of injection current, the BAL exhibits an increased near-field size with a rate of about 8.3 μm A^{-1}. Although the growing thermal lens leads to near-field width shrinkage of each lateral mode, it will also activate an additional mode of higher order in combination with the increasing current crowding near the stripe edges. Therefore, the rising number of lateral lasing modes results in increased near-field size. On the other hand, the original near-field size of the STL is considerably larger,[26)] which shrinks first up to 2 A, then increases. At low current, this expanded near field of the STL may be attributed to light scattering from the microstructures, which results in additional emission beyond the stripe. As the optical field of low-order mode shrinks due to the growing thermal lens and high-order modes are suppressed, the overlap of the optical mode with the etched microstructures reduces, leading to initial near-field narrowing with increasing current. However, higher-order modes may take part in lasing due to enhanced index guiding and current crowding near the contact edges at high current. Therefore, the near-field width of the STL increases slightly at the next

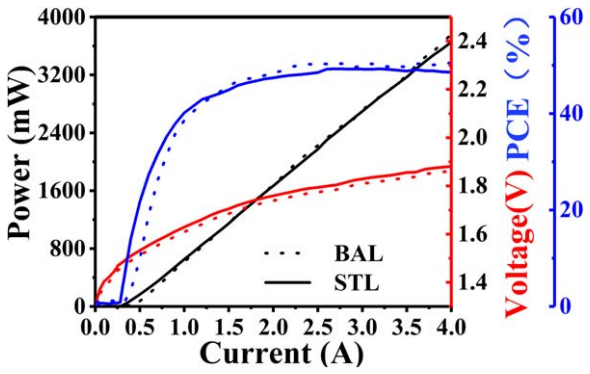

Fig. 3. (Color online) Optical power, voltage and conversion efficiency versus current for the STL (solid line) and BAL (dash line) at 20 °C.

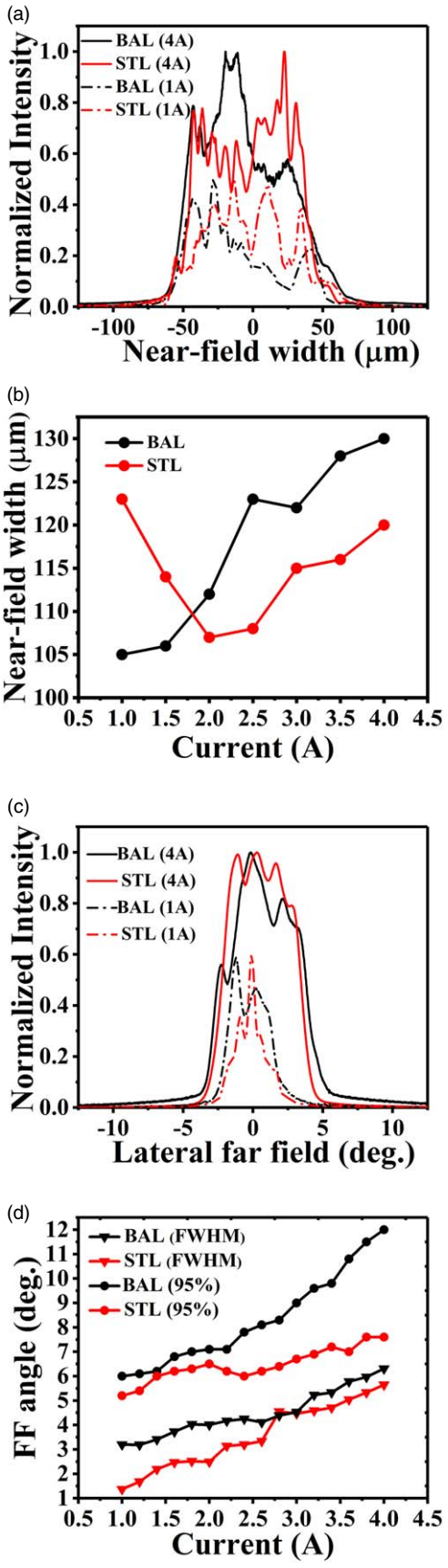

Fig. 4. (Color online) (a), (b) Measured near-field profiles at 1 A/4 A, and near-field widths (95% power) versus the injection current of the STL and BAL. (c), (d) Comparison of measured lateral far-field profiles at 1 A/4 A, and far-field (FF) angles versus the injection current of the STL and BAL.

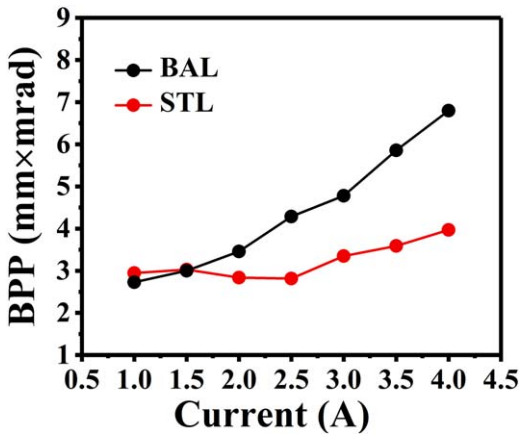

Fig. 5. (Color online) Lateral beam quality of the STL and BAL at different injection currents under CW operation.

current step.[30] However, the STL still shows a narrower near field than the BAL up to 4 A.

The corresponding lateral divergence angles (measured by BP209-VIS Beam Profiler) at different currents are plotted in Figs. 4(c) and 4(d) for the BAL and STL. As can be seen, the BAL exhibits a strong far-field blooming with increasing current. Its far-field angle is 3.2° (FWHM) and 6° (95% power inclusion) at 1 A current, which rapidly broadens to 6.3° (FWHM) and 12° (95% power inclusion) at 4 A. In contrast, the STL shows improved far-field behavior, which exhibits a narrower and more stable lateral far field (especially for 95% power inclusion) than the BAL. The lateral divergence angle of the STL is only 1.37° (FWHM) and 5.2° (95% power inclusion) at 1 A current and slightly increases to 5.6° (FWHM) and 7.6° (95% power inclusion) at 4 A. The far-field angles in the definition of FWHM for both kinds of lasers are very close, which indicates that lower-order lateral modes are less influenced by the loss-tailoring area. Furthermore, the obviously reduced far-field angle (95% power contained) is strong evidence for a reduced number of lasing modes after the implementation of loss tailoring. This demonstrates that the microstructures can delay the appearance of high-order lateral modes.

The lateral beam parameter product (BPP) is quantified based on the measured near-field width and far-field angle with 95% of the total power content. In Fig. 5, experimental results for lateral beam qualities at various currents are compared for both kinds of lasers. As can be seen, their BPP values are more or less equal at low currents up to 1.5 A, but differ significantly for higher currents. For the BAL, more lateral modes join in lasing with increasing current, leading to a rapid increase of BPP with a rate of 1.5 mm × mrad A^{-1}. The STL exhibits a clear improvement of the beam quality over the reference BAL at high currents, which is very stable up to 2.5 A and then degrades at a much slower rate. The improvement is directly linked to the reduced mode number by the introduction of sawtooth microstructures, which provides more loss for high-order modes. In this case, only lower-order modes will allow lasing and hence the deterioration of the beam quality under high current is suppressed. At 4 A, the BPP value of the STL is reduced from 6.9 mm × mrad to 4 mm × mrad by a factor as high as 42%. The corresponding lateral brightness improves by about 68%, which can be further optimized to achieve better performance.

In conclusion, we have presented an approach to improve the beam quality of broad-area diode lasers with the assistance of etched sawtooth microstructures, which provide more propagation loss for high-order modes. Thanks to such selective loss tailoring, the structured lasers show less dependence on the injection current for the far-field divergence and BPP value. The lateral beam quality improves by 42% due to the reduced number of guided lateral modes. Furthermore, the near field of low-order lateral modes shrinks with increasing current due to the thermal lens effect, which leaves less mode power in the lossy region. Therefore, such self-adjusting modal loss results in hardly any power and efficiency degradation. By further optimization in the microstructure parameters and current injection pattern, higher brightness can be expected. This technique provides an easy method to develop high-beam-quality diode laser while maintaining high power and high efficiency output.

Acknowledgments This work was supported by the National Natural Science Foundation of China (Grant Nos. 61761136009 and 61774153), the Jilin Provincial Foundation (Grant No. 20190302053GX), the National Defense Science and Technology Key Laboratory Foundation (Grant No. 6142107190309) and the Opened Fund of the State Key Laboratory of High Power Semiconductor Laser.

1) Y. Inoue and S. Fujikawa, IEEE J. Quantum Electron. **36**, 751 (2000).
2) O. G. Okhotnikov and F. M. Aranjo, IEEE Photonics Technol. Lett, **6**, 933 (1994).
3) C. X. Yu, O. Shatrovoy, T. Y. Fan, and T. F. Taunay, Opt. Lett. **41**, 5202 (2016).
4) N. Shimada, M. Yukawa, K. Shibata, K. Ono, T. Yagi, and A. Shima, Proc. SPIE **7198**, 719806 (2009).
5) L. Li, Opt. Lasers Eng. **34**, 231 (2000).
6) Q. Gaimard, M. Triki, T. Nguyen-Ba, L. Cerutti, G. Boissier, R. Teissier, A. Baranov, Y. Rouillard, and A. Vicet, Opt. Express **23**, 19118 (2015).
7) A. Pietrzak, M. Zorn, R. Huelsewede, J. Meusel, and J. Sebastian, Proc. SPIE **10900**, 109000K (2019).
8) Y. Kaifuchi, Y. Yamagata, R. Nogawa, R. Morohashi, Y. Yamada, and M. Yamaguchi, Proc. SPIE **10086**, 100860D (2017).
9) P. Kirkby, A. Goodwin, G. Thompson, and P. Selway, IEEE J. Quantum Electron. **13**, 705 (1977).
10) A. I. Bawamia, B. Eppich, K. Paschke, H. Wenzel, F. Schnieder, G. Erbert, and G. Tränkle, Appl. Phys. B **97**, 95 (2009).
11) M. Winterfeldt, P. Crump, H. Wenzel, G. Erbert, and G. Tränkle, J. Appl. Phys. **116**, 063103 (2014).
12) J. Piprek, Proc. SPIE **8619**, 861910 (2013).
13) J. Piprek and Z. M. Simon Li, Appl. Phys. Lett. **102**, 221110 (2013).
14) M. Winterfeldt, P. Crump, S. Knigge, A. Maabdorf, U. Zeimer, and G. Erbert, IEEE Photonics Technol. Lett. **27**, 1809 (2015).
15) J. G. Bai et al., Proc. SPIE **7953**, 79531F (2011).
16) H. Wenzel, P. Crump, J. Fricke, P. Ressel, and G. Erbert, IEEE J. Quantum Electron. **49**, 1102 (2013).
17) T. Wang, L. Wang, S. Shu, S. Tian, Z. Zhao, C. Tong, and L. Wang, Chin. Opt. Lett. **15**, 071404 (2017).
18) P. Salet, F. Gerard, T. Fillion, A. Pinquier, J. Gentner, S. Delepine, and P. Doussiere, IEEE Photonics Technol. Lett. **10**, 1706 (1998).
19) T. Wang, C. Tong, L. Wang, Y. Zeng, S. Tian, S. Shu, J. Zhang, and L. Wang, Appl. Phys. Express **9**, 112102 (2016).
20) J. P. Hohimer, D. C. Craft, G. A. Vawter, and D. R. Myers, Appl. Phys. Lett. **58**, 2886 (1991).
21) G. Sobczak, E. Dabrowska, M. Teodorczyk, K. Krzyzak, and A. Malag, IEEE J. Quantum Electron. **50**, 890 (2014).
22) G. Sobczak, E. Dąbrowska, M. Teodorczyk, J. Kalbarczyk, and A. Maląg, Proc. SPIE **8702**, 87020B (2013).
23) X. Zhou, X. Ma, H. Qu, A. Qi, Z. Chen, Y. Wang, and W. Zheng, Appl. Phys. Express **12**, 094004 (2019).
24) L. Liu, H. Qu, Y. Wang, Y. Liu, Y. Zhang, and W. Zheng, Opt. Lett. **39**, 3231 (2014).

25) C. H. Tsai, Y. S. Su, C. W. Tsai, D. P. Tsai, and C. F. Lin, IEEE Photonics Technol. Lett. **16**, 2412 (2004).
26) M. J. Miah, S. Strohmaier, G. Urban, and D. Bimberg, Appl. Phys. Lett. **113**, 22 (2018).
27) P. Crump et al., Appl. Phys. Lett. **92**, 131113 (2008).
28) L. Wang, C. Tong, S. Shu, S. Tian, F. Sun, Y. Zhao, H. Lu, X. Zhang, G. Hou, and L. Wang, Opt. Lett. **44**, 3562 (2019).
29) C. Zink, M. Niebuhr, A. Jechow, A. Heuer, and R. Menzel, Opt. Express **22**, 14108 (2014).
30) J. Piprek, IEEE Photonics Technol. Lett. **25**, 958 (2013).